Validation of a Compensation Strategy Used to Detect Choriocapillaris Flow Deficits Under Drusen With Swept Source OCT Angiography

YINGYING SHI, ZHONGDI CHU, LIANG WANG, QINQIN ZHANG, WILLIAM FEUER, LUIS DE SISTERNES, MARY K. DURBIN, GIOVANNI GREGORI, RUIKANG K. WANG, AND PHILIP J. ROSENFELD

• PURPOSE: **A compensation strategy that was developed to measure the choriocapillaris (CC) flow deficits (FDs) under drusen was tested in eyes with large drusen from age-related macular degeneration (AMD) before and after the drusen spontaneously resolved without evidence of disease progression.**

• DESIGN: **Prospective, observational consecutive case series.**

• METHODS: **Patients with AMD were enrolled in a prospective swept-source optical coherence tomography (SS-OCT) imaging study. Consecutive eyes with large drusen were followed, and eyes that underwent spontaneous collapse of drusen without evidence of disease progression were identified retrospectively. The drusen-resolved regions were manually outlined. CC FDs were measured using a previously published compensation strategy that adjusted for the decreased signal intensity underlying drusen. Both the percentage of FDs (FD%) and the mean FD sizes (MFDSs) were measured before and after drusen resolution.**

• RESULTS: **Resolution of drusen was identified in 8 eyes from 8 patients. The average interval between the 2 visits was 7.8 months. The average drusen volumes measured between visits were 0.23 and 0.04 mm^3, respectively. After the drusen resolved, the average follow-up time without evidence of disease progression was 10.1 months. When the 2 visits were compared, there were no statistically significant differences in any of the CC parameters within the drusen resolved regions once the compensation strategy was applied (all *P* values $>.22$).**

• CONCLUSIONS: **In this naturally occurring experiment in which drusen collapsed without evidence of disease progression, the CC parameters were similar once our compensation strategy was applied both before and after the drusen resolved. (Am J Ophthalmol 2020;220: 115–127. © 2020 Elsevier Inc. All rights reserved.)**

Accepted for publication Jun 19, 2020.

From the Department of Ophthalmology, Bascom Palmer Eye Institute, University of Miami Miller School of Medicine (Y.S., L.W., W.F., G.G., P.J.R.), Miami, FL; Department of Bioengineering, University of Washington (Z.C., Q.Z., R.K.W.), Seattle, Washington; and Research and Development, Carl Zeiss Meditec, Inc (L.d.S., M.K.D.), Dublin, California, USA.

Inquiries to Philip J. Rosenfeld, Bascom Palmer Eye Institute, 900 NW 17th Street, Miami, FL 33136, USA; e-mail: prosenfeld@miami.edu

THE CHORIOCAPILLARIS (CC) IS A DENSE MONOLAYER meshwork of fenestrated capillaries within the choroid adjacent to the Bruch membrane (BM) that provides nutritional support for the retinal pigment epithelium (RPE) and outer retina.[1] Histologic studies have shown that a decrease in CC density is associated with normal aging and age-related macular degeneration (AMD).[2–5] Ramrattan and associates found a decrease in CC density in eyes with drusen and geographic atrophy (GA).[2] Mullins and associates studied 21 donor eyes diagnosed with early AMD and found that the CC vessel density was significantly decreased under drusen compared with age-matched normal eyes.[4] Up until recently, the study of the CC in vivo could not be routinely performed using conventional imaging techniques such as fluorescein angiography and indocyanine green angiography because of the small caliber of the capillaries, the small intercapillary spacing, and the overlying RPE, which prevents direct visualization of the CC using dye-based angiography.[6]

With the development of spectral domain optical coherence tomography angiography (SD-OCTA) and swept source OCTA (SS-OCTA), the CC can be visualized in vivo and longitudinal studies have been performed.[7–22] SS-OCTA provides the best visualization of the CC because of the longer wavelength (1060 nm) of its light source compared with SD-OCTA imaging at a wavelength of 840 nm.[23] The longer wavelength used by SS-OCTA instruments allows for better penetration of the light through the RPE and the longer wavelength is safer, so a higher laser energy can be used to provide a better signal-to-noise ratio and improved visualization of the CC.[23] In addition, the faster scanning rate of the SS-OCTA instruments allows for denser scanning patterns for a given acquisition time, which results in improved image quality. The ability of OCTA to detect blood flow within the CC is achieved by repeating multiple B-scans at a specific position and then using specific algorithms that compare differences in the intensity and phase signals from these repeated B scans. These differences are considered to be the result of erythrocytes moving within the capillaries; thus, these changes in the signals from repeated B-scans represent blood flow.[17,24]

Using SS-OCTA imaging, several groups using high resolution research instruments have reported changes in the CC that are consistent with previously published histologic

0002-9394/$36.00
https://doi.org/10.1016/j.ajo.2020.06.033

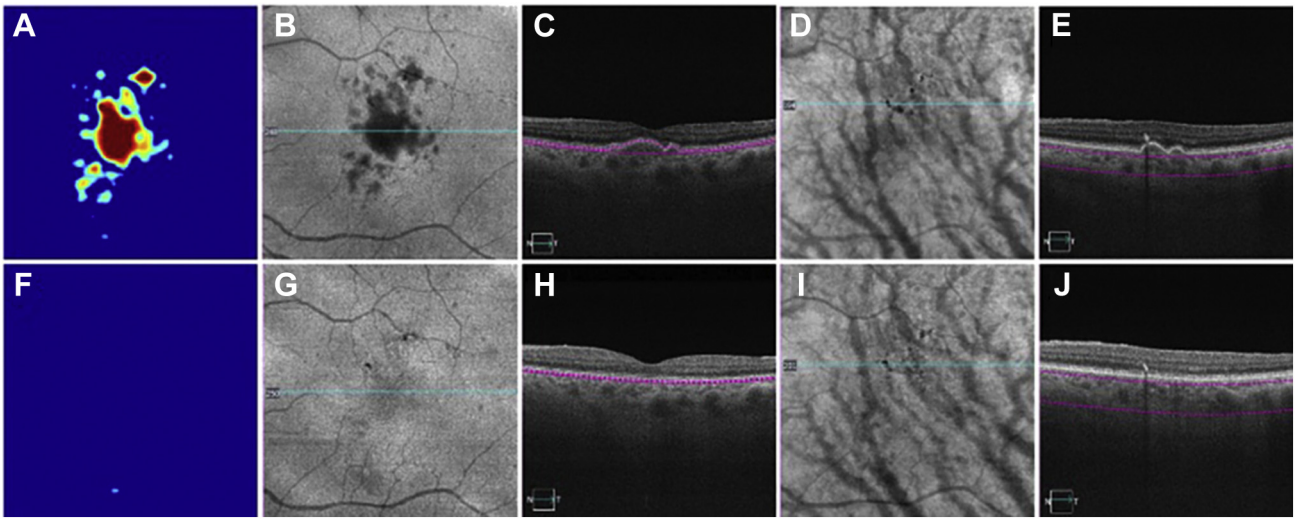

FIGURE 1. An eye with drusen imaged by swept source optical coherence tomography angiography (SS-OCTA) before and after the collapse of drusen. These images correspond to case 2 shown in Tables 1 and 2. A-E. Images before drusen collapse. F-J. Images after drusen collapse. A, F. Drusen volume maps before (0.18 mm^3) and after drusen collapse (0.00 mm^3), respectively. B, G. The en face structure images using a custom slab segmented from the retinal pigment epithelium (RPE) to the Bruch membrane (BM). The hyporeflectivity area corresponds to the drusen area as shown in B before drusen collapsed. The area of hyporeflectivity corresponding to drusen was disappeared as drusen resolved shown in G. C, H. Corresponding B-scans showing drusen caused RPE elevation before drusen collapse (G), and the RPE elevation was flattened as drusen resolved (H). D, I. Pigmentation identified as black foci on en face structure images customized using a slab located from 64 to 400 μm below BM. E, J. Corresponding B-scans showing pigmentation as hyperreflective foci and causing hypotransmission onto the underlying choroid.

findings.[25–29] Although the lateral resolution of 14 to 20 μm obtained from other SS-OCTA instruments precludes the direct visualization of CC capillaries and lobules within the macular region compared with the peripheral regions, the resolution does allow for the detection of flow deficits (FDs) or regions within the capillary meshwork where the blood flow is undetectable and these FDs can be quantified.[7–17,19–23,30–35] Using SS-OCTA imaging, Zheng and associates investigated CC FDs in 164 normal eyes from different age groups,[7] and they found that CC FDs increased with age, especially within the central 1-mm circle under the fovea, which is consistent with previous histologic findings,[2] and other SS-OCTA reports.[16,31]

Several groups have attempted to study the CC in AMD, and while an increase in macular CC FDs was reported, these groups were unable to quantitate the CC FDs under drusen because of the signal attenuation and the shadowing effect of drusen on the underlying choroid, especially when SD-OCTA was used.[13,15,22] Nassisi and associates followed 46 eyes with drusen using SD-OCTA for a minimum of 1 year, and they demonstrated an inability to detect the CC under drusen.[15] However, they did find significant CC impairment around drusen, and this impairment appeared to be associated with the appearance and growth of drusen, which suggested that changes in the CC might play an important role in disease progression.

Even though SS-OCTA, with its longer wavelength, has been shown to be better than SD-OCTA in identifying CC flow impairment under drusen,[23] the larger drusen can still cast a shadow on the underlying CC. Zhang and associates developed a strategy to compensate for this signal attenuation caused by drusen.[36] This compensation strategy uses the corresponding CC en face structural image. This en face structural image provides information on the signal level at each en face location, and this signal level can then be used to compensate for the attenuated flow signal at corresponding locations. During compensation, the structural image is first inverted so that the darker signal intensities under drusen become brighter. This enhanced signal intensity from the inverted image is then used to enhance the CC flow signal under drusen. This compensation strategy was tested on both normal eyes and drusen eyes, and while the quantitation of CC FDs remained the same in normal eyes without drusen, the CC was visualized better under drusen with this compensation strategy, and the repeatability of these measurements was improved. Several groups have used this strategy to visualize the CC in eyes with drusen secondary to AMD and have shown that drusen are associated with an increase in CC FDs.[11,12,15,32] However, uncertainty persists as to whether this increase in CC FDs under drusen is real or the result of an inability to fully compensate for the signal attenuation.

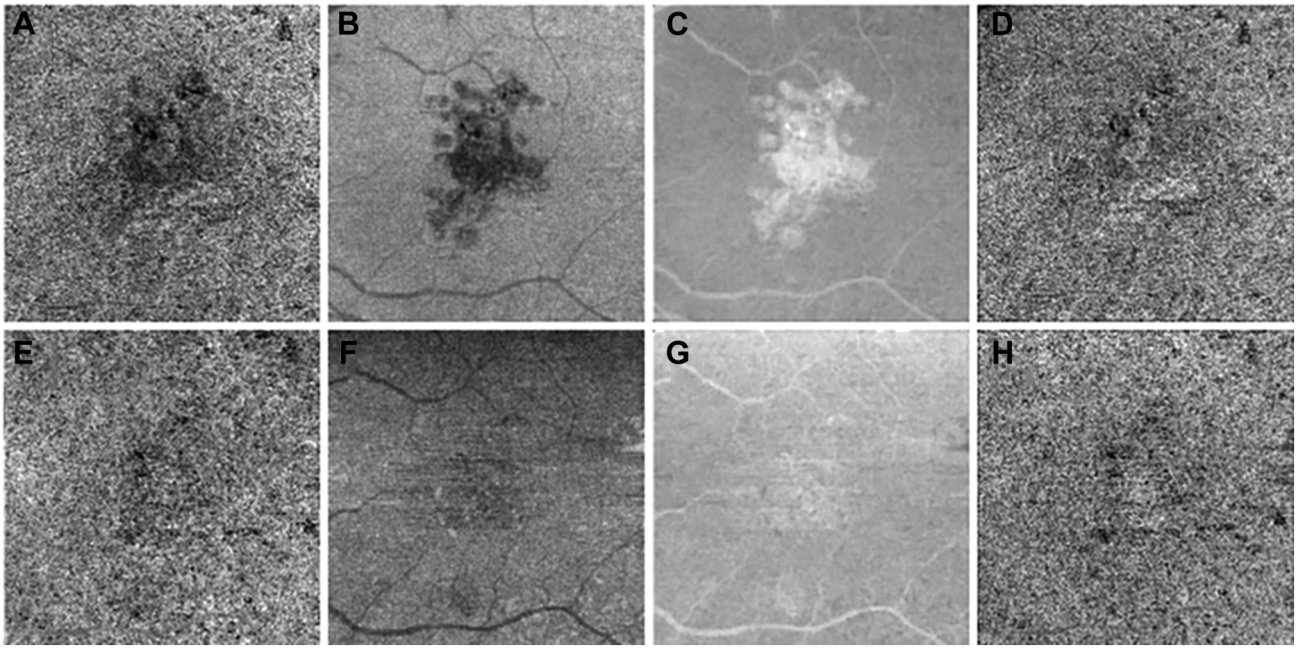

FIGURE 2. Compensation strategy used to enhance the choriocapillaris (CC) flow signal under drusen using swept source optical coherence tomography angiography (SS-OCTA). A-D. Images before drusen collapse. E-H. Images after drusen collapse. A, B, E, F. CC en face images using a custom slab of 15 μm thickness and located 16 μm below the Bruch membrane. A. The CC flow signal under drusen appears attenuated and corresponds to the hyporeflective area under drusen as shown in B. This signal attenuation disappeared after the drusen collapsed as shown in E and F. C, G. Inverted and smoothed en face CC structure images that were used to compensate A and E, respectively. D, H. Compensated CC en face flow images using C and G, respectively. The CC signal under drusen was enhanced whereas the signal in normal regions appeared similar.

To determine if our compensation strategy adequately corrects for the signal attenuation caused by drusen, we investigated the CC in eyes that had a significant drusen burden and then underwent a resolution of these drusen without any obvious anatomic changes that would suggest disease progression. Although infrequent, the resolution of drusen without any sequelae can occur as reported in our previous natural history studies.[37,38] The sequelae of interest include the formation of nascent geographic atrophy (nGA), also known as incomplete outer retina and RPE atrophy, GA, also known as complete outer retina and RPE atrophy, or macular neovascularization.[39,40] In this current report, we show that our strategy successfully compensated for the signal attenuation caused by drusen, and no obvious differences in the measurements of CC FDs were detected before and after the drusen collapsed.

PATIENTS AND METHODS

PATIENTS WERE ENROLLED IN A PROSPECTIVE SS-OCT IMAGing study approved by the institutional review board of the University of Miami Miller School of Medicine. Informed consent was obtained from each subject. The study was performed in accordance with the tenets of the Declaration of Helsinki and complied with the Health Insurance Portability and Accountability Act of 1996.

Patients with intermediate AMD having drusen volumes ≥0.03 mm^3 within a circle of radius 3 mm centered at the fovea were included in this study. Drusen volume was measured using a fully automated algorithm described in previous works.[37,41] These patients were followed prospectively using SS-OCTA imaging (PLEX Elite 9000; Carl Zeiss Meditec, Inc, Dublin, California, USA). None of these eyes had evidence of nGA or GA. Patients were imaged according to their routine clinical care schedule. Those eyes that subsequently showed resolution of drusen without formation of nGA, GA, or exudation were identified (Figure 1). SS-OCTA images from the 2 closest visits before and after drusen resolution were used for analysis of CC FDs.

SS-OCTA images were obtained using an SS-OCTA instrument with a scanning rate of 100,000 A-scans per second that had a swept source laser with a central wavelength of 1,060 nm, resulting in a full width at half maximum axial resolution of 5.0 μm in tissue and a lateral resolution of 20 μm estimated at the retinal surface. At least one 6 × 6-mm scan centered on the fovea was performed at each visit on each eye. Only scans with a signal strength of 7

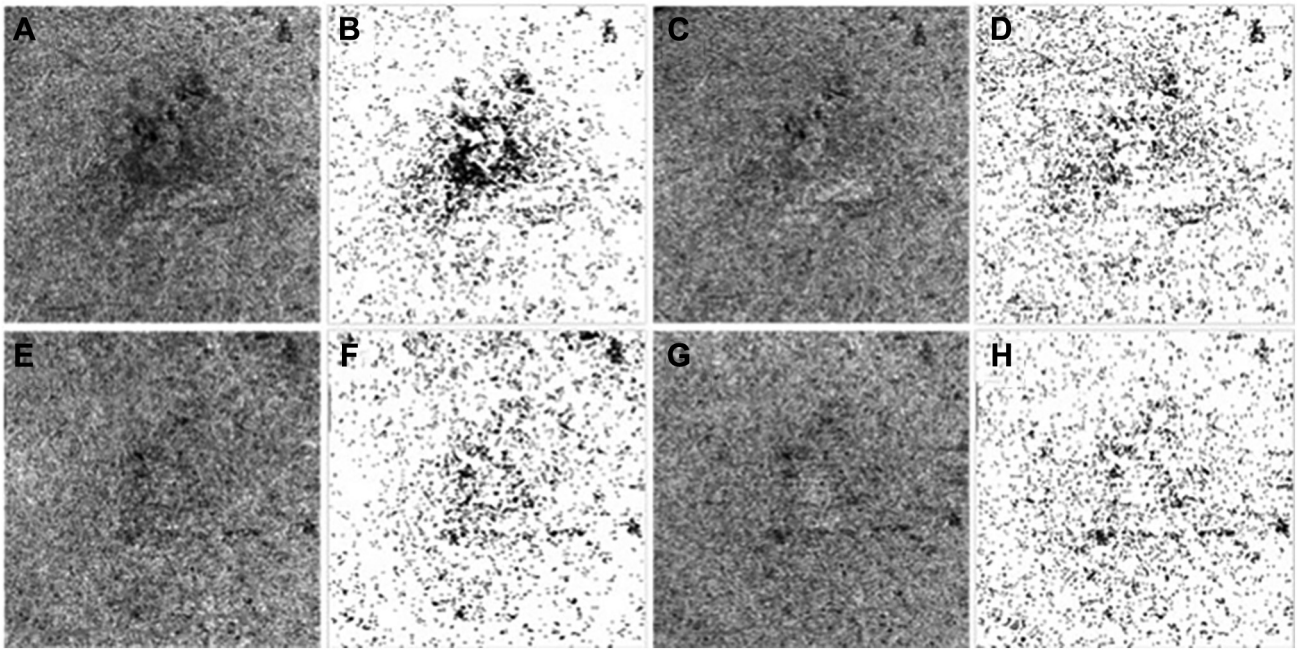

FIGURE 3. Fuzzy C means threshold method applied to the uncompensated and compensated choriocapillaris (CC) images before and after drusen collapse. A-D. Images before drusen collapse. E-H. Images after drusen collapse. A, E. Uncompensated CC en face flow images using a custom slab of 15 μm thickness and located 16 μm below the Bruch membrane. B, F. CC binary maps thresholded using Fuzzy C means based on uncompensated images (A, E). C, G. Compensated CC en face flow images using a validated compensation strategy. D, H. CC binary maps thresholded using Fuzzy C means method based on compensated images (C, G).

or greater without motion artifacts were retained. Each 6 × 6-mm scan consisted of 500 A-scans and 500 B-scans. Each B scan was repeated twice at the same position, resulting in a homogenous sampling grid with a separation of 12 μm. The detection of flow information was achieved using the complex optical microangiography (OMAG) algorithm.[42] The CC was visualized by creating an en face image summarizing the flow information using a 15-μm-thick slab that started from 16 μm below BM.[43] En face flow images were produced using a maximum projection method, which entailed taking the average of the 5 highest-valued pixels at each scan position within the slab limits, and the 6×6 mm images were resized into 1024 × 1024 pixels to be consistent with machine output images. After removal of the retinal projection artifacts,[44] a compensation strategy was applied to adjust for the signal attenuation due to drusen as previously described.[36] Briefly, the CC signal attenuation caused by the overlying drusen (Figure 2, A, B, E, and F) was compensated by using the inverted and smoothed CC en face structural image to amplify the signal under drusen (Figure 2, C and G). This resulted in a compensation of the shadowing seen on the CC en face flow image under drusen whereas the signal in the regions without drusen remained unchanged (Figures 2, D and H). Before the CC was analyzed, nonrigid registration was performed on retinal OCTA images before and after the drusen resolved so that the same transformation was applied onto CC en face flow images. In the next step, both uncompensated CC en face flow images (Figure 2, A and E) and compensated CC en face flow images (Figure 2, D and H) were thresholded and the CC FDs measured.

Two different thresholding methods were used in this study: the Fuzzy C means (FCM) method and the Phansalkar method. The FCM approach is a global thresholding method based on the histogram distribution of all intensities from all the pixels throughout the entire image.[45] All pixels were self-clustered into different clusters, where the number of clusters was automatically determined using the elbow method. All pixels clustered into the first cluster with the lowest OCTA intensities were then segmented as FDs. In contrast, the Phansalkar method is a local threshold strategy and was designed for analyzing images with low contrast.[43,46] Phansalkar thresholding is computed for each pixel within a certain window radius, and as such, the value of thresholding changes when choosing different window radii. Our previous studies have shown that when using the Phansalkar method and choosing a large window radius of 15 pixels, which equals 88 μm in a 6 × 6-mm image that was resized into1024 × 1024 pixels, the CC results appeared non-physiologic both qualitatively and quantitatively.[43] However, when a smaller window radius of 2 to 4 pixels was used, which equals 12 to 24 μm in a 6 × 6-mm scan measuring 1024 × 1024 pixels, the results appeared more physiologic and consistent with the FCM method when the CC was visualized and quantified.[43,46] Thus, in

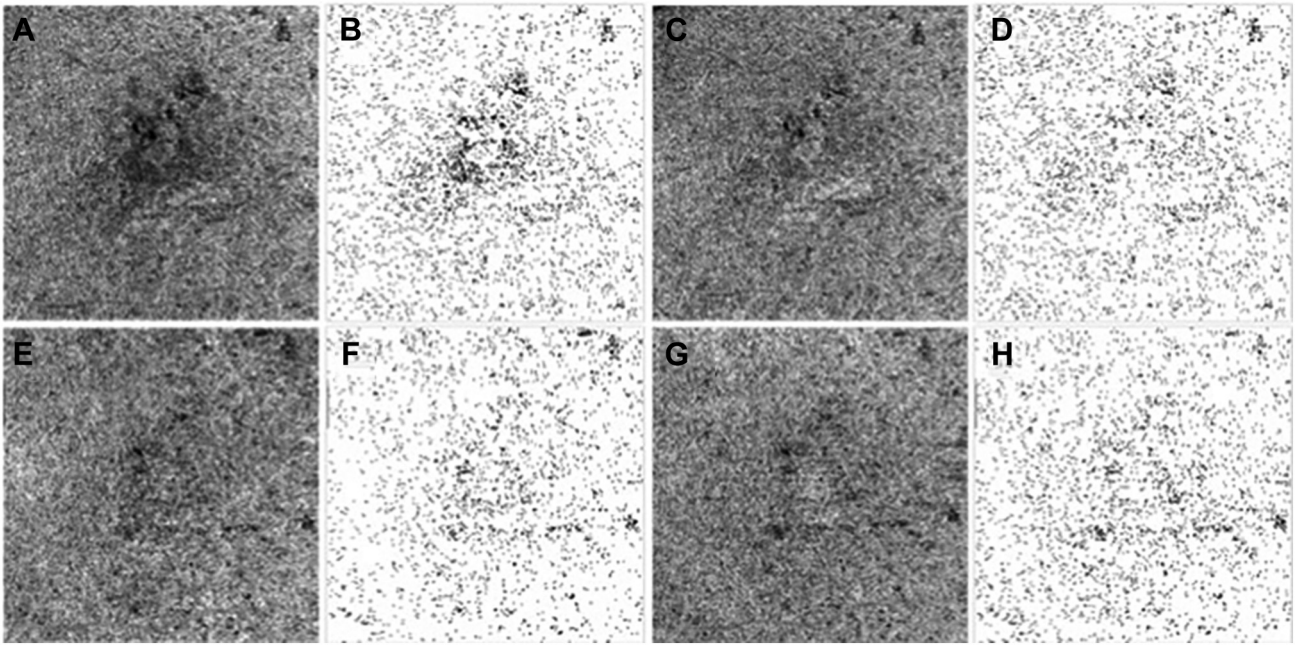

FIGURE 4. Phansalkar threshold method applied to the uncompensated and compensated choriocapillaris (CC) images before and after drusen collapse. A-D. Images before drusen collapse. E-H. Images after drusen collapse. A, E. Uncompensated CC en face flow images using a custom slab of 15 μm thickness and located 16 μm below the Bruch membrane. B, F. CC binary maps thresholded using Phansalkar method with an 18 μm window radius based on uncompensated images (A, E). C, G. Compensated CC en face flow images using a validated compensation strategy. D, H. CC binary maps thresholded using Phansalkar method with an 18 μm window radius based on compensated images (C, G).

this current study, we used both the FCM method and the Phansalkar method with a 3-pixel (18-μm) window radius to threshold the CC en face images. After thresholding, any FDs with an equivalent diameter smaller than 24 μm were removed because they were smaller than the average normal intracapillary distance and most likely represented speckle noise.[47] Overall, there were 4 different CC binary maps used for the final CC quantification: both uncompensated and compensated CC en face flow images thresholded using the FCM method (Figure 3) and uncompensated and compensated CC en face flow images thresholded using the Phansalkar method with an 18-μm window radius (Figure 4). The CC FD measurements were then compared between these images before and after the resolution of drusen.

At each visit, 2 regions were identified, and the CC FDs were quantified in these regions (Figure 5). The first region involved the area of drusen resolution (Figure 5, C and G). At each visit, we manually outlined the area of the drusen using the en face structure images created by a custom slab segmented from the RPE to BM. The resolved drusen area was generated by subtracting drusen outlines at the resolved visit from drusen outlines at the visit prior to resolution. The second region served as a control for CC quantitation between visits and consisted of a 300-μm-wide rim located 150 to 450 μm outside of all the drusen (Figure 5, D and H). This region should not have any signal attenuation from the drusen and should not have been affected by the resolution of the drusen. For each case, the CC FDs between 2 visits were compared within the resolved drusen area and within the rim area outside of all the drusen.

Another region of interest included the hyperreflective foci within the retina and foci of hyperpigmentation at the level of the RPE that cause complete blockage of the incident light, which is appreciated as hypotransmission defects on the underlying choroid. This blockage of signal cannot be compensated because the signal is totally absent and not just attenuated. Because we were unable to visualize the CC under these areas of hyperpigmentation, we excluded these regions from the CC analyses. To identify these areas of signal loss, we manually outlined areas of pigmentation with a greatest linear dimension of 125 μm or greater on customized en face structure images from each visit using a slab starting from 64 to 400 μm under BM and then we combined these areas of pigmentation from these 2 visits (Figure 5, B and F) and excluded them from the CC quantification at both visits (Figure 5, C, D, G, and H). A greatest linear dimension of at least 125 μm was chosen as a size that could be reproducibly identified and quantified by 2 independent graders. These 2 independent graders were involved in manually outlining the drusen and areas of pigment, and then consensus gradings were reached on all outlines. If there was disagreement

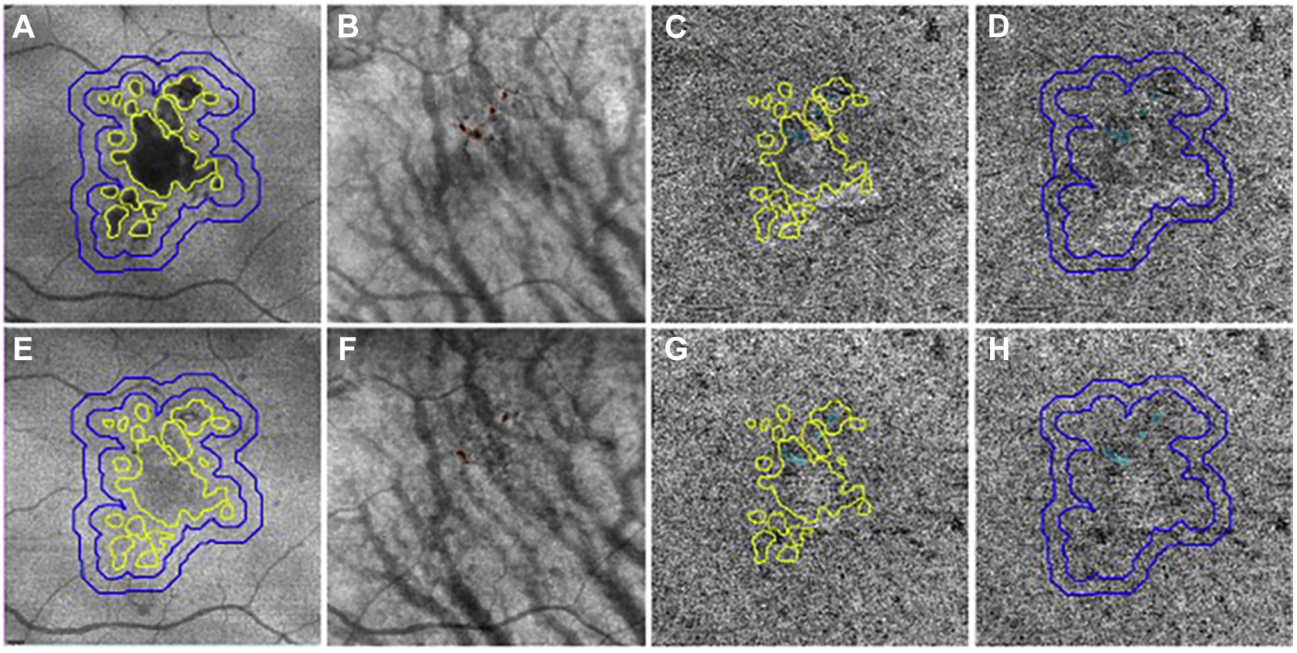

FIGURE 5. Choriocapillaris (CC) measurements performed in different regions before and after drusen collapse using swept source optical coherence tomography angiography (SS-OCTA). A-D. Images before drusen collapse. E-H. Images after drusen collapse. A, E. Custom en face structural images segmenting between the retinal pigment epithelium (RPE) and the Bruch membrane (BM) showing drusen and drusen collapsed. CC was analyzed in the resolved drusen area depicted by the yellow outlines. CC was also quantified in a 150- to 450-μm-rim region outside of all the drusen depicted by blue outlines. B, F. Pigmentation (red outlines) showing on custom en face structural images segmented from 64 to 400 μm under BM. C, G. resolved drusen area depicted as yellow outlines superimposed on compensated CC en face images and used for CC quantification. Teal color highlights pigmentation areas that were combined of red outlines from B and F. These areas were excluded from the final CC analysis. D, H. The rim region located 150 to 450 μm outside of all the drusen superimposed on the compensated CC en face flow images and used for CC quantification. Teal color highlights pigmentation areas that were a combination of red outlines from B and F. These areas were excluded from the final CC analysis.

that could not be resolved, then the dispute was adjudicated by a senior grader (P.J.R.).

Quantitative parameters used to assess FDs in this study includes FD percentage (FD%) and mean flow deficit size (MFDS). FD% was defined as the percentage of pixels representing FDs relative to all the pixels in the total analyzed area. MFDS was defined as the average area of individual FDs in the analyzed area.

Statistical analyses were performed using MATLAB (issue R2016b; Math Works, Inc, Natick, Massachusetts, USA). Descriptive statistics were reported as mean and standard deviation (SD). Statistical significance of differences between means were assessed with the paired *t* test. *P* values smaller than .05 were considered statistically significant.

RESULTS

A TOTAL OF 128 CONSECUTIVE EYES WITH DRUSEN SECONDARY to intermediate AMD were enrolled and followed. Eight eyes from 8 patients were found to undergo resolution of drusen without formation of nGA, GA, or exudation. One patient had drusen that partially collapsed between 2 different intervals. As a result, 9 visits were included in this study. The average age of these patients was 67.9 (SD: 2.5) years, and 62.5% of them were women. The mean of drusen volume at their baseline visit was 0.23 mm^3 (SD: 0.27; median: 0.12 mm^3, range: 0.04-0.86 mm^3). The mean of drusen volume at the visit when drusen resolved was 0.04 mm^3 (SD: 0.03; median: 0.04 mm^3, range: 0.00-0.98 mm^3). The average follow-up time from baseline to drusen resolution was 7.8 months (SD: 3.8; median: 6.84 months, range: 2.8-14.5 months). After drusen resolution, we kept following these patients for an average of 10.1 months (SD: 8.5; median: 8.8 months, range: 0.0-20.5 months). Except 2 patients who were lost to follow-up after drusen resolved, none of the other eyes developed nGA, GA, or exudation.

When using the uncompensated CC images before and after drusen resolution and comparing the regions of drusen resolution and the rim regions using the FCM thresholding approach, we found a significant difference in the CC FD% measurements within the drusen-resolved region between

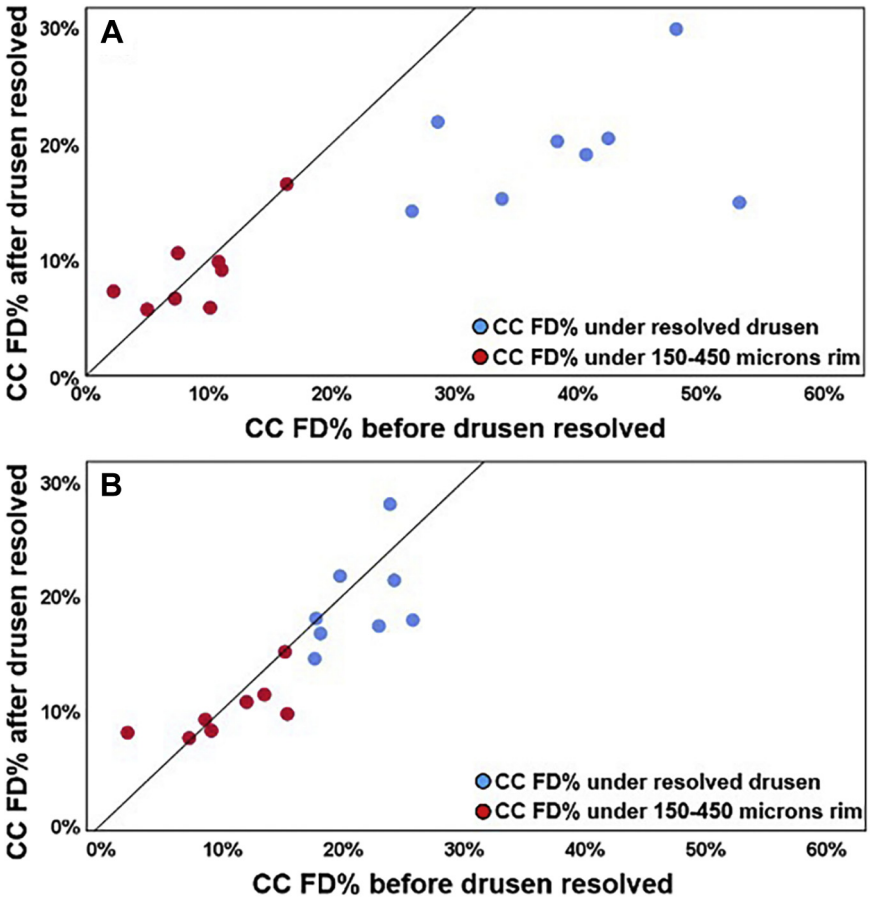

FIGURE 6. Comparison of choriocapillaris (CC) flow deficit percentage (FD%) from different regions before and after drusen resolution using uncompensated and compensated CC images that were thresholded using Fuzzy C means method. A. CC FD% analysis using uncompensated images before and after drusen resolution. A significant difference in CC FD% was found within the drusen-resolved region ($P = .001$) between 2 visits, whereas the CC FD% in the rim region between 2 visits showed no difference ($P = .890$), as only the red dots are scattered evenly around the line of unity. B. CC FD% analysis using compensated images before and after drusen resolution. No significant difference in CC FD% was found in both the drusen-resolved region and the rim region, $P = .22$ and .7, respectively, as both the red dots and the blue dots are scattered evenly around the line of unity.

the 2 visits ($P = .001$), but there was no significant difference in the rim region ($P = .89$), as shown in Figure 6, A. Once the compensation strategy was applied, there were no significant differences before and after resolution in either the drusen-resolved region ($P = .22$) or the rim region ($P = .70$), as shown in Figure 6, B, and Table 1. Similarly, when using the uncompensated CC images before and after drusen resolution and comparing the regions of drusen resolution and the rim regions using the Phansalkar thresholding approach, we found a significant difference in the CC FD% measurements within the drusen-resolved region between the 2 visits ($P = .025$), but there was no significant difference in the rim region ($P = .494$), as shown in Figure 7, A. Once the compensation strategy was applied, there were no significant differences before and after resolution in either the drusen-resolved region ($P = .283$) or the rim region ($P = .578$), as shown in Figure 7, B, and Table 2.

Similar outcomes were observed when comparing the CC MFDS measurements as shown in Figures 8 and 9. When using uncompensated images thresholded with the FCM method, we found a significant difference in the CC MFDS measurements within the drusen-resolved region between the 2 visits ($P = .003$), but there was no significant difference in the rim region ($P = .88$), as shown in Figure 8, A. Once the compensation strategy was applied, there were no significant differences before and after resolution in either the drusen-resolved region ($P = .511$) or the rim region ($P = .815$), as shown in Figure 8, B. When using uncompensated images thresholded with the Phansalkar method, we found a significant difference in the CC MFDS measurements within the drusen-resolved region between the 2 visits ($P = .024$), but there was no significant difference in the rim region ($P = .863$), as shown in Figure 9, A. Once the compensation strategy was applied, there were no significant differences before and after

TABLE 1. Choriocapillaris Flow Deficits Measurements Using Compensated Images Thresholded by Fuzzy C Means Method Before and After Drusen Resolved

	CC FD% Before Drusen Resolved		CC FD% After Drusen Resolved		CC MFDS Before Drusen Resolved, mm^2		CC MFDS After Drusen Resolved, mm^2	
Case No.	Under Resolved Drusen	Under a Rim Area Outside of Drusen	Under Resolved Drusen	Under a Rim Area Outside of Drusen	Under Resolved Drusen	Under a Rim Area Outside of Drusen	Under Resolved Drusen	Under a Rim Area Outside of Drusen
1	19.70	15.14	21.63	15.01	0.0232	0.0271	0.0205	0.0237
2	18.08	15.34	16.61	9.59	0.0146	0.0110	0.0113	0.0083
3	17.71	8.56	17.92	9.14	0.0180	0.0117	0.0205	0.0132
4	26.20	7.09	15.19	7.99	0.0249	0.0114	0.0232	0.0134
5	25.24	7.33	20.37	6.77	0.0234	0.0122	0.0284	0.0132
6	24.18	13.45	21.26	11.28	0.0248	0.0167	0.0280	0.0169
7	17.59	1.89	14.41	7.45	0.0274	0.0082	0.0178	0.0133
8	23.83	11.96	27.90	10.62	0.0264	0.0168	0.0253	0.0155
9	22.92	9.02	17.27	8.12	0.0164	0.0142	0.0175	0.0152

CC = choriocapillaris; FD% = flow deficit percentage; MFDS = mean flow deficit size.

resolution in either drusen-resolved region ($P = .346$) or the rim region ($P = .494$), as shown in Figure 9, B.

In general, when either the FCM or Phansalkar thresholding methods were used, the differences between visits in the drusen-resolved regions were statistically significant without compensation (Figures 6A, 7A, 8A, and 9A), but when the compensation strategy was applied, there were no differences in the CC FD measurements in the drusen-resolved areas when the 2 visits were compared using either thresholding strategy (Figures 6B, 7B, 8B, and 9B). In the rim regions, there were no differences in the CC measurements with or without compensation (Figures 6-9). Of note, as shown in Figures 6 to 9 and in Tables 1 and 2, the compensated FD% and MFDS measurements were larger under the drusen-resolved region compared with the rim regions, and these differences were all statistically significant (all P values $< .02$), but whether these differences are due to the relative location of the CC within the central macula versus the rim region or associated with the formation of drusen remains to be determined and is under active investigation.

DISCUSSION

USING A NATURALLY OCCURRING EXPERIMENT IN WHICH drusen spontaneously resolved, we have been able to show that our strategy to adjust for signal attenuation under drusen adequately compensated for the signal loss and allowed us to visualize and measure the CC FDs under drusen. No significant differences in CC FD measurements in the areas of resolved drusen were observed before and after drusen resolution when we used this previously published compensation strategy. Moreover, this compensation strategy had little effect on the rim region outside the drusen, which is consistent with the expected behavior of the algorithm. With the results of this study, we can now follow the natural history of CC FDs in eyes with AMD knowing that our compensation strategy appears to give us reliable information, but the values may be different depending on the thresholding strategy used. However, as long as the same thresholding strategy is used for all CC analyses within a given study, this should not be a problem. These results give us increased confidence that we can now use this compensation strategy when studying the role of CC perfusion abnormalities in AMD disease progression.

We also studied the impact of this compensation strategy on the rim region outside the drusen. In the absence of drusen, the compensation strategy had no effect on the rim region. However, there were statistically significant differences between the CC measurements under the drusen regions compared with the rim regions. These differences between the rim regions and the resolved drusen regions were to be expected based on the topologic distribution of CC FD changes expected with age. We previously showed that CC impairment is more prominent under the central foveal region compared with the outer macular regions as we age.[7] Moreover, these results are consistent with both previous histopathologic and SS-OCTA studies reporting decreased CC flow measurements under drusen when our compensation strategy was used.[12,48] Whether the preferential loss of CC perfusion under drusen is significantly different from the age-related loss expected in regions with similar topographical distributions in age-matched controls remains to be determined. If drusen are associated with the loss of CC perfusion, then it also remains to be determined if the loss of CC perfusion precedes the formation of drusen or whether drusen result in the

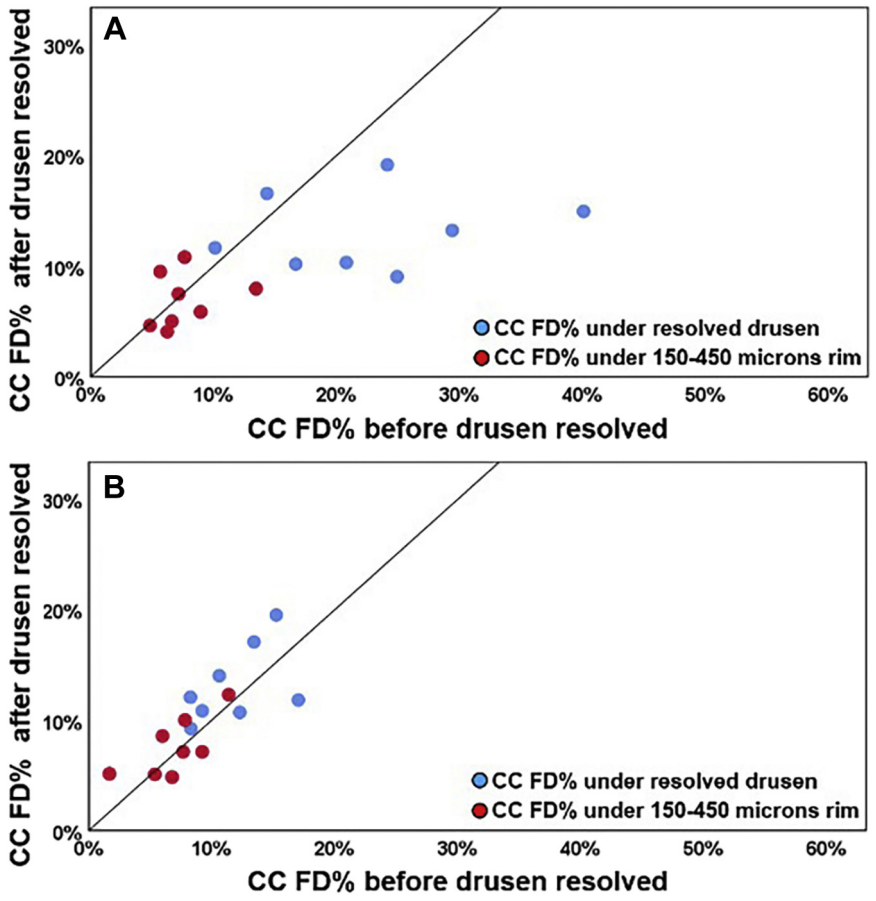

FIGURE 7. Comparison of choriocapillaris (CC) flow deficit percentages (FD%) from different regions before and after drusen resolution using uncompensated and compensated CC images which were thresholded using Phansalkar method with an 18 μm window radius. A. CC FD% analysis using uncompensated images before and after drusen resolution. A significant difference in CC FD% was found within the drusen-resolved region ($P = .025$) between 2 visits, whereas the CC FD measures in the rim region showed no difference ($P = .494$), as only the red dots are scattered evenly around the line of unity. B. CC FD% analysis using compensated images before and after drusen resolution. No significant difference in CC FD% were found in both the drusen-resolved region and the rim region, $P = .283$ and .578, respectively, as both the red dots and the blue dots are scattered evenly around the line of unity.

preferential loss of CC perfusion. Although Borelli and associates[12] suggest that CC loss precedes the formation of drusen, these authors used a CC slab that was deeper in the choroid than our slab and they used the Phansalkar thresholding strategy with a window radius of 15 pixels (88 μm), which resulted in nonphysiologic FD measurements as shown in our previous work.[43,46] This type of longitudinal study needs to be repeated using an appropriately positioned CC slab and either the FCM or the Phansalkar 3-pixel (18-μm) radius thresholding approach.

In our current report, we not only demonstrated the validity of our compensation strategy but also demonstrated similar results using either the FCM or Phansalkar thresholding strategies, as long as the window radius for the Phansalkar method was 18 μm. Previously, Chu and associates compared the FCM and Phansalkar thresholding methods using normal eyes and drusen eyes and they found that the FCM method was similar to the Phansalkar method when analyzing the CC FDs as long as the window radius was appropriately chosen.[43,46] Unlike many previous studies that chose a default window radius of 88 μm without any justification,[10,19,32,34,49–51] Chu and associates provided the rationale for choosing a radius dependent on the characteristics of the processed CC en face image, and in our current study, we chose a radius of 18 μm and our results were similar to the results using the FCM method, which is consistent with their previous findings. However, we want to emphasize that the actual CC FDs values were slightly different when using different thresholding methods. It remains to be determined which of the thresholding methods produce results that are closest to the ground truth, but as our imaging hardware and software improves, we will eventually be able to answer that question. In the

TABLE 2. Choriocapillaris Flow Deficits Measurements Using Compensated Images Thresholded by Phansalkar Method With an 18-μm Window Radius Before and After Drusen Resolved

Case No.	CC FD% Before Drusen Resolved		CC FD% After Drusen Resolved		CC MFDS Before Drusen Resolved, mm^2		CC MFDS After Drusen Resolved, mm^2	
	Under Resolved Drusen	Under a Rim Area Outside of Drusen	Under Resolved Drusen	Under a Rim Area Outside of Drusen	Under Resolved Drusen	Under a Rim Area Outside of Drusen	Under Resolved Drusen	Under a Rim Area Outside of Drusen
1	8.25	7.81	12.05	9.98	0.0011	0.0128	0.0094	0.0107
2	9.21	9.21	10.82	7.11	0.0009	0.0081	0.0096	0.0078
3	10.59	5.98	14.00	8.54	0.0010	0.0077	0.0109	0.0085
4	17.50	6.60	10.05	5.06	0.0117	0.0081	0.0127	0.0079
5	16.54	6.92	13.56	4.60	0.0106	0.0084	0.0138	0.0085
6	15.22	11.36	19.50	12.28	0.0110	0.0104	0.0172	0.0126
7	8.30	1.67	9.20	5.12	0.0113	0.0060	0.0102	0.0084
8	13.41	7.66	17.06	7.11	0.0141	0.0096	0.0111	0.0086
9	12.27	5.36	10.69	5.08	0.0089	00083	0.0105	0.0093

CC = choriocapillaris; FD% = flow deficit percentage; MFDS = mean flow deficit size.

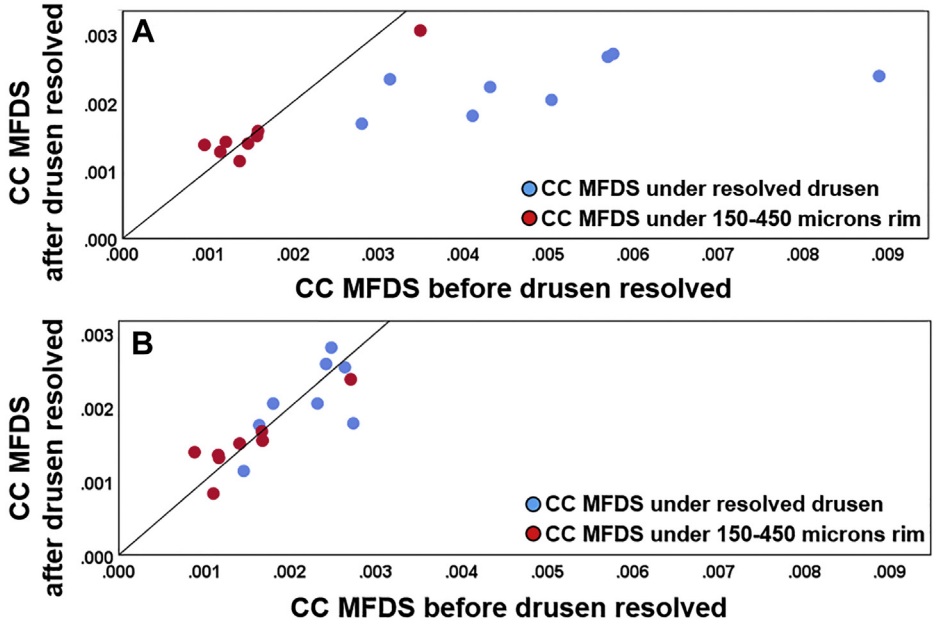

FIGURE 8. Comparison of choriocapillaris (CC) mean flow deficit size (MFDS) from different regions before and after drusen resolution using uncompensated and compensated CC images that were thresholded using Fuzzy C means method. A. CC MFDS analysis using uncompensated images before and after drusen resolution. A significant difference in the CC MFDS was found within the drusen-resolved region ($P = .003$) between 2 visits, whereas the CC MFDS in the rim region showed no difference ($P = .88$), as only the red dots are scattered evenly around the line of unity. B. CC MFDS analysis using compensated images before and after drusen resolution. No significant difference in the CC MFDS measurements were found in both the drusen-resolved region and the rim region, $P = .511$ and .815, respectively, as both the red dots and the blue dots are scattered evenly around the line of unity.

meantime, as long as an investigator uses the same appropriate thresholding strategy while studying disease progression, then the results describing relative changes in CC FDs should be valid.

Although the compensation strategy was successful in adjusting for the signal attenuation under drusen so that the CC FDs could be adequately measured in these cases, we do not know the limits of this compensation strategy. At some point, the drusen may be so large that the signal attenuation is too great to compensate. This extreme situation is best demonstrated not by the drusen but by the presence of pigment clumps or plaques that appear as OCT-

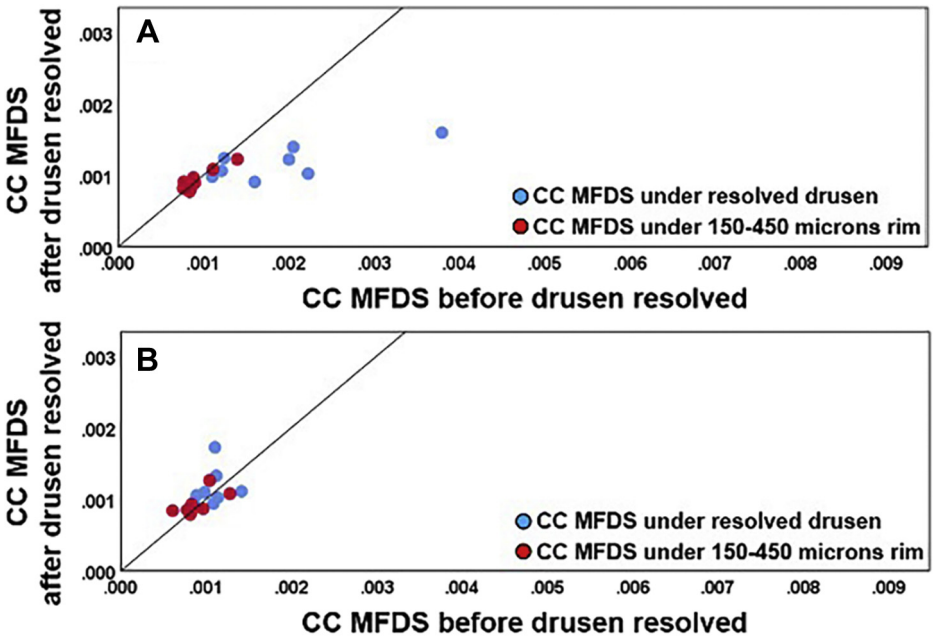

FIGURE 9. Comparison of choriocapillaris (CC) mean flow deficit size (MFDS) from different regions before and after drusen resolution using uncompensated and compensated CC images that were thresholded using Phansalkar method with an 18 μm window radius. A. CC MFDS analysis using uncompensated images before and after drusen resolution. A significant difference in CC MFDS was found within the drusen-resolved region ($P = .024$) between 2 visits, whereas the CC MFDS measurements in the rim region showed no difference ($P = .863$), as only the red dots are scattered evenly around the line of unity. B. CC MFDS analysis using compensated images before and after drusen resolution. No significant difference in the CC MFDS measurements were found in both the drusen-resolved region and the rim region, $P = .346$ and .494, respectively, as both the red dots and the blue dots are scattered evenly around the line of unity.

defined hyperreflective material in the retina or at the level of the RPE.[39,52] Both of these types of lesions result in complete blockage of the incident light with distinct areas of hypotransmission detected in the choroid.[39] These areas of hypotransmission are easily captured on en face choroidal images that are segmented under the BM, the same slab that is used to visualize the hypertransmission seen in areas of GA.[39] In this current study, we used this slab as described in the Methods section, and we were able to detect these areas of pigmentation as black foci on the en face structural images, and these black areas corresponded to the areas of hypotransmission seen on B-scans (Figure 1, E and J). Any areas of pigmentation with a greatest linear dimension larger than 125 μm were identified either before or after the drusen resolved, and these combined areas were excluded from the CC analyses because they could not be compensated because of the complete physical loss of the choroidal signal. Although this article describes our technical quantitative strategy for signal compensation, the fundamental concept of using the structural image to identify areas of signal attenuation before attempting to assess the validity of any flow image is vitally important when interpreting any OCT angiographic image.

The limitations of our current study include the small sample size and the variable follow-up. As we previously reported, the small sample size was to be expected given the rarity of drusen resolution without any sequalae, which is approximately 4% per year, so the 8 eyes out of the 128 cases reviewed is what we would have expected.[37] Although the follow-up was variable, the visit intervals were close enough together so that we did not observe any significant changes in the control rim region. This rim region not only served as a control for the algorithm but also as a control for possible age-related changes that might have occurred between visits. Another limitation is that we also lacked the in vivo ground truth regarding the status of CC FDs in eyes with drusen. It should be mentioned that the use of this compensation strategy alters the intensity distribution in the compensated images and may affect features that could be important for other types of analyses, such as certain forms of machine learning. Despite these limitations, our results in this study are encouraging and help set the stage for further explorations of this topic.

In summary, this current study showed that our compensation strategy for the attenuated signal under drusen successfully adjusted for the diminished signal under drusen as shown by our ability to obtain similar results before and after the drusen resolved. We also accumulated additional evidence to support the use of either a global or local thresholding strategy as long as appropriate parameters are

chosen for whichever algorithm is used. This knowledge will allow us to apply these strategies in future studies as we investigate the role of CC perfusion deficits in AMD disease progression.

FUNDING/SUPPORT: THIS RESEARCH WAS SUPPORTED BY GRANTS FROM THE NATIONAL EYE INSTITUTE (R01EY024158, R01EY028753), Carl Zeiss Meditec, Inc (Dublin, California, USA), the Salah Foundation, an unrestricted grant from the Research to Prevent Blindness, Inc, New York, NY, and the National Eye Institute Center Core Grant (P30EY014801) to the Department of Ophthalmology, University of Miami Miller School of Medicine. The funding organizations had no role in the design or conduct of this research. Financial Disclosures: Giovanni Gregori, Ruikang K. Wang, and Philip J. Rosenfeld received research support from Carl Zeiss Meditec, Inc. Giovanni Gregori and the University of Miami co-own a patent that is licensed to Carl Zeiss Meditec, Inc. Philip J. Rosenfeld also receives additional research funding from Stealth Bio Therapeutics. He is also a consultant for Apellis, Biogen, Boehringer-Ingelheim, Carl Zeiss Meditec, Chengdu Kanghong Biotech, EyePoint, Ocunexus Therapeutics, Ocudyne, and Unity Biotechnology. He also has equity interest in Apellis, Valitor, Verana Health, and Ocudyne. Ruikang K. Wang discloses intellectual property owned by the Oregon Health and Science University and the University of Washington. He also receives research support from Tasso Inc, Moptim Inc, Colgate Palmolive Company, and Facebook technologies LLC. He is a consultant to Insight Photonic Solutions, Kowa, and Carl Zeiss Meditec. The remaining authors have no disclosures. All authors attest that they meet the current ICMJE criteria for authorship.

REFERENCES

1. Nickla DL, Wallman J. The multifunctional choroid. *Prog Retin Eye Res* 2010;29:144–168.
2. Ramrattan RS, van der Schaft TL, Mooy CM, de Bruijn WC, Mulder PG, de Jong PT. Morphometric analysis of Bruch's membrane, the choriocapillaris, and the choroid in aging. *Invest Ophthalmol Vis Sci* 1994;35:2857–2864.
3. Lengyel I, Tufail A, Hosaini HA, Luthert P, Bird AC, Jeffery G. Association of drusen deposition with choroidal intercapillary pillars in the aging human eye. *Invest Ophthalmol Vis Sci* 2004;45:2886–2892.
4. Mullins RF, Johnson MN, Faidley EA, Skeie JM, Huang J. Choriocapillaris vascular dropout related to density of drusen in human eyes with early age-related macular degeneration. *Invest Ophthalmol Vis Sci* 2011;52:1606–1612.
5. Biesemeier A, Taubitz T, Julien S, Yoeruek E, Schraermeyer U. Choriocapillaris breakdown precedes retinal degeneration in age-related macular degeneration. *Neurobiol Aging* 2014;35:2562–2573.
6. Pauleikhoff D, Spital G, Radermacher M, Brumm GA, Lommatzsch A, Bird AC. A fluorescein and indocyanine green angiographic study of choriocapillaris in age-related macular disease. *Arch Ophthalmol* 1999;117:1353–1358.
7. Zheng F, Zhang Q, Shi Y, et al. Age-dependent changes in the macular choriocapillaris of normal eyes imaged with swept-source optical coherence tomography angiography. *Am J Ophthalmol* 2019;200:110–122.
8. Shi Y, Zhang Q, Zheng F, et al. Correlations between different choriocapillaris flow deficit parameters in normal eyes using swept source OCT angiography. *Am J Ophthalmol* 2020;209:18–26.
9. Thulliez M, Zhang Q, Shi Y, et al. Correlations between choriocapillaris flow deficits around geographic atrophy and enlargement rates based on swept-source OCT imaging. *Ophthalmol Retina* 2019;3:478–488.
10. Borrelli E, Shi Y, Uji A, et al. Topographic analysis of the choriocapillaris in intermediate age-related macular degeneration. *Am J Ophthalmol* 2018;196:34–43.
11. Moult EM, Waheed NK, Novais EA, et al. Swept-source optical coherence tomography angiography reveals choriocapillaris alterations in eyes with nascent geographic atrophy and drusen-associated geographic atrophy. *Retina* 2016;36:S2–S11.
12. Borrelli E, Uji A, Sarraf D, Sadda SR. Alterations in the choriocapillaris in intermediate age-related macular degeneration. *Invest Ophthalmol Vis Sci* 2017;58:4792–4798.
13. Chatziralli I, Theodossiadis G, Panagiotidis D, Pousoulidi P, Theodossiadis P. Choriocapillaris vascular density changes in patients with drusen: cross-sectional study based on optical coherence tomography angiography findings. *Ophthalmol Ther* 2018;7:101–107.
14. Choi W, Moult EM, Waheed NK, et al. Ultrahigh-speed, swept-source optical coherence tomography angiography in nonexudative age-related macular degeneration with geographic atrophy. *Ophthalmology* 2015;122:2532–2544.
15. Nassisi M, Tepelus T, Nittala MG, Sadda SR. Choriocapillaris flow impairment predicts the development and enlargement of drusen. *Graefes Arch Clin Exp Ophthalmol* 2019;257:2079–2085.
16. Al-Sheikh M, Falavarjani KG, Pfau M, Uji A, Le PP, Sadda SR. Quantitative features of the choriocapillaris in healthy individuals using swept-source optical coherence tomography angiography. *Ophthalmic Surg Lasers Imaging Retina* 2017;48:623–631.
17. Choi W, Mohler KJ, Potsaid B, et al. Choriocapillaris and choroidal microvasculature imaging with ultrahigh speed OCT angiography. *PLoS One* 2013;8:e81499.
18. Chu Z, Chen CL, Zhang Q, et al. Complex signal-based optical coherence tomography angiography enables in vivo visualization of choriocapillaris in human choroid. *J Biomed Opt* 2017;22:1–10.
19. Nassisi M, Baghdasaryan E, Tepelus T, Asanad S, Borrelli E, Sadda SR. Topographic distribution of choriocapillaris flow deficits in healthy eyes. *PLoS One* 2018;13:e0207638.
20. Waheed NK, Moult EM, Fujimoto JG, Rosenfeld PJ. Optical coherence tomography angiography of dry age-related macular degeneration. *Dev Ophthalmol* 2016;56:91–100.
21. Borrelli E, Mastropasqua R, Senatore A, et al. Impact of choriocapillaris flow on multifocal electroretinography in intermediate age-related macular degeneration eyes. *Invest Ophthalmol Vis Sci* 2018;59:AMD25–AMD30.
22. Chatziralli I, Theodossiadis G, Panagiotidis D, Pousoulidi P, Theodossiadis P. Choriocapillaris' alterations in the presence of reticular pseudodrusen compared to drusen: study based on OCTA findings. *Int Ophthalmol* 2018;38:1887–1893.
23. Lane M, Moult EM, Novais EA, et al. Visualizing the choriocapillaris under drusen: comparing 1050-nm swept-source

versus 840-nm spectral-domain optical coherence tomography angiography. *Invest Ophthalmol Vis Sci* 2016;57:585–590.
24. Kim DY, Fingler J, Zawadzki RJ, et al. Optical imaging of the chorioretinal vasculature in the living human eye. *Proc Natl Acad Sci U S A* 2013;110:14354–14359.
25. Kurokawa K, Liu Z, Miller DT. Adaptive optics optical coherence tomography angiography for morphometric analysis of choriocapillaris [Invited]. *Biomed Opt Express* 2017;8:1803–1822.
26. Kurokawa K, Sasaki K, Makita S, Hong YJ, Yasuno Y. Three-dimensional retinal and choroidal capillary imaging by power Doppler optical coherence angiography with adaptive optics. *Opt Express* 2012;20:22796–22812.
27. Gorczynska I, Migacz JV, Jonnal R, Zawadzki RJ, Poddar R, Werner JS. Imaging of the human choroid with a 1.7 MHz A-scan rate FDML swept source OCT system. SPIE; 2017:10.
28. Migacz JV, Gorczynska I, Azimipour M, Jonnal R, Zawadzki RJ, Werner JS. Megahertz-rate optical coherence tomography angiography improves the contrast of the choriocapillaris and choroid in human retinal imaging. *Biomed Opt Express* 2019;10:50–65.
29. Zhou K, Song S, Zhang Q, Chu Z, Huang Z, Wang RK. Visualizing choriocapillaris using swept-source optical coherence tomography angiography with various probe beam sizes. *Biomed Opt Express* 2019;10:2847–2860.
30. Nassisi M, Shi Y, Fan W, et al. Choriocapillaris impairment around the atrophic lesions in patients with geographic atrophy: a swept-source optical coherence tomography angiography study. *Br J Ophthalmol* 2019;103:911–917.
31. Sacconi R, Borrelli E, Corbelli E, et al. Quantitative changes in the ageing choriocapillaris as measured by swept source optical coherence tomography angiography. *Br J Ophthalmol* 2019;103:1320–1326.
32. Spaide RF. Choriocapillaris flow features follow a power law distribution: implications for characterization and mechanisms of disease progression. *Am J Ophthalmol* 2016;170:58–67.
33. Spaide RF. Optical coherence tomography angiography signs of vascular abnormalization with antiangiogenic therapy for choroidal neovascularization. *Am J Ophthalmol* 2015;160:6–16.
34. Spaide RF. Choriocapillaris signal voids in maternally inherited diabetes and deafness and in pseudoxanthoma elasticum. *Retina* 2017;37:2008–2014.
35. Zhang Q, Chen CL, Chu Z, et al. Automated quantitation of choroidal neovascularization: a comparison study between spectral-domain and swept-source OCT angiograms. *Invest Ophthalmol Vis Sci* 2017;58:1506–1513.
36. Zhang Q, Zheng F, Motulsky EH, et al. A novel strategy for quantifying choriocapillaris flow voids using swept-source OCT angiography. *Invest Ophthalmol Vis Sci* 2018;59:203–211.
37. Yehoshua Z, Wang F, Rosenfeld PJ, Penha FM, Feuer WJ, Gregori G. Natural history of drusen morphology in age-related macular degeneration using spectral domain optical coherence tomography. *Ophthalmology* 2011;118:2434–2441.
38. Schaal KB, Rosenfeld PJ, Gregori G, Yehoshua Z, Feuer WJ. Anatomic clinical trial endpoints for nonexudative age-related macular degeneration. *Ophthalmology* 2016;123:1060–1079.
39. Guymer RH, Rosenfeld PJ, Curcio CA, et al. Incomplete retinal pigment epithelial and outer retinal atrophy in age-related macular degeneration: classification of atrophy meeting report 4. *Ophthalmology* 2020;127:394–409.
40. Sadda SR, Guymer R, Holz FG, et al. Consensus definition for atrophy associated with age-related macular degeneration on OCT: Classification of Atrophy Report 3. *Ophthalmology* 2018;125:537–548.
41. Gregori G, Wang F, Rosenfeld PJ, et al. Spectral domain optical coherence tomography imaging of drusen in nonexudative age-related macular degeneration. *Ophthalmology* 2011;118:1373–1379.
42. Wang RK, An L, Francis P, Wilson DJ. Depth-resolved imaging of capillary networks in retina and choroid using ultrahigh sensitive optical microangiography. *Opt Lett* 2010;35:1467–1469.
43. Chu Z, Gregori G, Rosenfeld PJ, Wang RK. Quantification of choriocapillaris with optical coherence tomography angiography: a comparison study. *Am J Ophthalmol* 2019;208:111–123.
44. Zhang A, Zhang Q, Wang RK. Minimizing projection artifacts for accurate presentation of choroidal neovascularization in OCT micro-angiography. *Biomed Opt Express* 2015;6:4130–4143.
45. Chu Z, Zhang Q, Zhou H, et al. Quantifying choriocapillaris flow deficits using global and localized thresholding methods: a correlation study. *Quant Imaging Med Surg* 2018;8:1102–1112.
46. Chu Z, Cheng Y, Zhang Q, et al. Quantification of choriocapillaris with Phansalkar local thresholding: pitfalls to avoid. *Am J Ophthalmol* 2020;213:161–176.
47. Zhang Q, Shi Y, Zhou H, et al. Accurate estimation of choriocapillaris flow deficits beyond normal intercapillary spacing with swept source OCT angiography. *Quant Imaging Med Surg* 2018;8:658–666.
48. Vujosevic S, Toma C, Villani E, et al. Quantitative choriocapillaris evaluation in intermediate age-related macular degeneration by swept-source optical coherence tomography angiography. *Acta Ophthalmol* 2019;97:e919–e926.
49. Borrelli E, Souied EH, Freund KB, et al. Reduced choriocapillaris flow in eyes with type 3 neovascularization and age-related macular degeneration. *Retina* 2018;38:1968–1976.
50. Uji A, Balasubramanian S, Lei J, Baghdasaryan E, Al-Sheikh M, Sadda SR. Choriocapillaris imaging using multiple en face optical coherence tomography angiography image averaging. *JAMA Ophthalmol* 2017;135:1197–1204.
51. Rochepeau C, Kodjikian L, Garcia MA, Mathis T. Optical coherence tomography angiography quantitative assessment of choriocapillaris blood flow in central serous chorioretinopathy. *Am J Ophthalmol* 2019;201:82–83.
52. Lujan BJ, Rosenfeld PJ, Gregori G, et al. Spectral domain optical coherence tomographic imaging of geographic atrophy. *Ophthalmic Surg Lasers Imaging* 2009;40:96–101.